

Article

Synthetic and Post-Synthetic Strategies to Improve Photoluminescence Quantum Yields in Perovskite Quantum Dots

ChaeHyun Lee ^{1,†} , Soo Jeong Lee ^{1,†} , YeJi Shin ¹ , Yeonsu Woo ¹ , Sung-Hwan Han ^{2,3},
Andrés Fabián Gualdrón-Reyes ^{4,*} , Iván Mora-Seró ⁴  and Seog Joon Yoon ^{1,*} 

¹ Department of Chemistry, College of Natural Science, Yeungnam University, 280 Daehak-Ro, Gyeongbuk, Gyeongsan 38541, Korea; dwuos@naver.com (C.L.); dltnwjd0102@naver.com (S.J.L.); aashinyj@naver.com (Y.S.); dndustn19@naver.com (Y.W.)

² Department of Chemistry, College of Natural Sciences, Hanyang University, Seoul 04763, Korea; shhan@hanyang.ac.kr

³ Luminano. Co., 222, Wangsimri-Ro, Seongdong-gu, Seoul 04763, Korea

⁴ Institute of Advanced Materials (INAM), Universitat Jaume I (UJI), Avenida de Vicent Sos Baynat s/n, 12071 Castelló de la Plana, Castellón, Spain; sero@uji.es

* Correspondence: gualdrón@uji.es (A.F.G.-R.); yoon@yu.ac.kr (S.J.Y.)

† These authors are equally contributed to this work.



Citation: Lee, C.; Lee, S.J.; Shin, Y.; Woo, Y.; Han, S.-H.; Gualdrón-Reyes, A.F.; Mora-Seró, I.; Yoon, S.J. Synthetic and Post-Synthetic Strategies to Improve Photoluminescence Quantum Yields in Perovskite Quantum Dots. *Catalysts* **2021**, *11*, 957. <https://doi.org/10.3390/catal11080957>

Academic Editors: Vignesh Kumaravel and Misook Kang

Received: 4 July 2021

Accepted: 2 August 2021

Published: 10 August 2021

Publisher's Note: MDPI stays neutral with regard to jurisdictional claims in published maps and institutional affiliations.



Copyright: © 2021 by the authors. Licensee MDPI, Basel, Switzerland. This article is an open access article distributed under the terms and conditions of the Creative Commons Attribution (CC BY) license (<https://creativecommons.org/licenses/by/4.0/>).

Abstract: Making high-quality raw materials is the key to open the versatile potential of next generation materials. All-inorganic CsPbX₃ (X: Cl[−], Br[−], and/or I[−]) perovskite quantum dots (PQDs) have been applied in various optoelectronic devices, such as photocatalysis, hydrogen evolution, solar cells, and light-emitting diodes, due to their outstanding photophysical properties, such as high photoluminescence quantum yield (PLQY), absorption cross-section, efficient charge separation, and so on. Specifically, for further improvement of the PLQY of the PQDs, it is essential to diminish the non-radiative charge recombination processes. In this work, we approached two ways to control the non-radiative charge recombination processes through synthetic and post-synthetic processes. Firstly, we proposed how refinement of the conventional recrystallization process for PbI₂ contributes to higher PLQY of the PQDs. Secondly, after halide exchange from CsPbI₃ PQDs to CsPbBr₃, through an in situ spectroelectrochemical setup, we monitored the positive correlation between bromide deposition of on the surface of the perovskite and photoluminescence improvement of the CsPbBr₃ perovskite film through electrodeposition. These two strategies could provide a way to enhance the photophysical properties of the perovskites for application to various perovskite-based optoelectronic devices.

Keywords: perovskite; perovskite quantum dots; recrystallization; electrodeposition; photoluminescence quantum yield

1. Introduction

The ABX₃ hybrid perovskites (A = MA⁺, FA⁺, and Cs⁺, where MA⁺: methylammonium, FA⁺: formamidinium, B = Pb²⁺ and Sn²⁺, and X = Cl[−], Br[−], and I[−]) with various dimensions (0D to 3D) have been widely studied for application to various optoelectronic devices, especially for boosting photoconversion efficiency of the perovskite-based solar cell up to 25.17% [1–3]. In the perovskite-based research field, using high-purity precursors is widely accepted among researchers for better photophysical properties such as high photoluminescence quantum yield (PLQY) for perovskite quantum dots (PQDs), high absorption cross-section, efficient charge separation, and advanced device performance [4–6]. To enhance the photoconversion efficiency, numerous strategies have been proposed but a major strategy is reducing photogenerated free carrier loss in the device [5–7]. The major reasons of current loss could be as follows: (1) free carrier trapping in the perovskite at various internal/surface

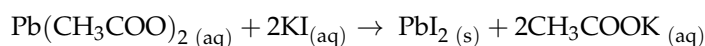
defects [5,8,9], (2) interfacial charge accumulation between the perovskite/charge transfer materials [10], and/or (3) insufficient charge transfer and regeneration processes [11,12]. To increase the efficient electron/hole separation and photoinduced current generation, researchers have been focused on decreasing surface defects by increasing grain size [8,13,14], surface defect passivation [15], applying recrystallization process of as-synthesized perovskite to reduce impurity to reduce internal defects [4], and so on. In the perovskite, various defects were studied but halide-based defects are easily formed due to their low defect formation energies [16]. Therefore, decreasing halide-induced defects in the perovskite is one of the important strategies for their better photophysical properties and efficient perovskite-based device performance.

In this work, we focused on the early stage, how the conventional recrystallization process for perovskite precursors affects the photophysical performance of the PQDs. Additionally, we figured out the role of the halide compositions to control the non-radiative recombination rate constant (k_{nr}) to enhance photophysical performances of the PQDs. Through in situ photoluminescence (PL) measurement with and without applied bias, we also observed that the post-synthetic process also provided a positive effect on increasing PLQY. Enriched halide surface passivation through electrodeposition could also be the key to increase PLQY through decreasing k_{nr} . The findings could also initiate how the halide plays an important role to the perovskites for application to various optoelectronic devices, such as light-emitting diodes (LEDs), solar cells, photocatalysis, hydrogen evolution reactions, and so on.

2. Results and Discussion

2.1. Impact of Recrystallization of PbI_2 Precursor for Photophysical Properties of the PQDs

To study the impact of the internal defect in the PQDs to their photophysical properties, we firstly focused on the most frequently used PQD, $CsPbI_3$ PQDs, and even various chemicals which were applied in the hot-injection method to synthesize the $CsPbI_3$ PQDs (details in Materials and Methods), we focused on one of the most important precursors, PbI_2 , which affects 1. stoichiometry and 2. halide-mediated defects in $CsPbI_3$ PQDs. To specify the role of purification, adapting motivation from our earlier work [6], we used the “Golden Rain” method (see Figure S1, provided by the Royal Society of Chemistry [17]) to obtain precipitation of PbI_2 , reaction scheme is as follows:



Additionally, we performed the recrystallization process with varying cooling rates (two different cooling rates, 2.38 h^{-1} and 0.690 h^{-1} , for Ice Bath and Hot Water PbI_2 , respectively) to observe the role of recrystallization on purity and I/Pb stoichiometry. In Figure 1A, X-ray diffraction (XRD) patterns of various PbI_2 are presented. Comparing the patterns to the pattern obtained from commercially available PbI_2 with 99% purity, synthesized and consecutive recrystallized XRD patterns present clear patterns, following hexagonal PbI_2 with P-3 mL space group (PDF# 04-007-2640). Compared to another XRD pattern from commercially available PbI_2 with 99.999% purity, the XRD patterns demonstrated identical PbI_2 XRD patterns without pattern from expected impurities, such as PbO , $PbCO_3$, and so on (see Figure S2). More details are under investigation to clarify the detailed chemical environment but through X-ray fluorescence (XRF) elemental analysis (Table S1), we were able to clarify that the recrystallized Ice Bath and Hot Water PbI_2 demonstrated the most similar stoichiometry (I/Pb ratio of 2.012 for Ice Bath and 2.000 for Hot Water) compared to As-synthesized and Commercial PbI_2 (2.059 and 2.016, respectively). We speculate that better stoichiometry between I and Pb is essential to avoid excess halide-based defects, such as iodide interstitials in the perovskite, which are easily formed under excess iodide (I-rich) conditions in the perovskite with lower defect formation energy as 0.19 eV over than valence band maximum [16,18,19]. Note that compared to our previous report [6], current I/Pb ratios (2.000–2.059) were shown to contain relatively smaller I/Pb ratios than early reported values (2.15–2.19). Relatively

smaller I/Pb ratios could be detrimental for controlling iodide mediated vacancies in the perovskite but in case of relatively smaller I/Pb conditions, the iodide interstitials could be one of the most critical factors to impact the non-radiative recombination process [16,18,19]. To summarize, we were able to obtain better PbI_2 through recrystallization without any impurity XRD patterns with better I/Pb stoichiometry that finally increased the optical performance of the PQDs synthesized with it.

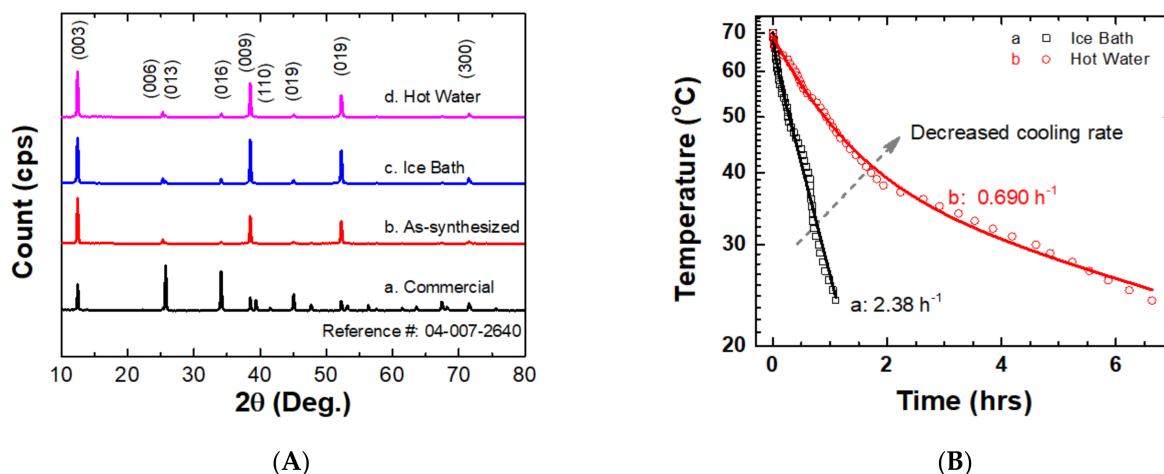


Figure 1. (A) XRD patterns of various PbI_2 a: commercially available, called here “Commercial”, b: as-synthesized, without recrystallization, called here “As-synthesized”, c: from as-synthesized PbI_2 , following the recrystallization process with rapid cooling in an ice bath, called here “Ice Bath”, d: from as-synthesized PbI_2 , following the recrystallization process with slower cooling in a bath containing 70 °C warm water, called here “Hot Water”. (B) Rapid and slow cooling rate of PbI_2 containing solutions in the two crystallization processes (Hot Water and Ice Bath), following the “Golden Rain” procedure [17].

Figure 2A presents UV-Vis. absorption spectrum of the CsPbI_3 PQDs with an absorption band edge at 665 nm and corresponds to the PL spectrum with a peak position at 685 nm. Around a 20 nm stoke shift was observed due to the relaxation of the vibration process to the valence band maximum in the PQD. The shift is reproducible compared to previously reported values [1]. With dependence on crystalline core size of the CsPbI_3 PQDs, due to the quantum confinement effect, the absorption band edge and emission peak shift could occur [1], but in this report, PQDs made using the four PbI_2 (Commercial, As-synthesized, Ice Bath, and Hot Water PbI_2) demonstrated negligible absorption band edge/emission peak position differences (see Figure S3). Furthermore, in Figure 2B, crystallized CsPbI_3 PQDs with around 7 to 9 nm cubic shapes were observed. In Figure S4, the size similarity can be observed by comparing PQDs made using the four PbI_2 , within their size distributions. Due to their similar sizes of PQDs, even using different PbI_2 for the PQD synthesis, we were able to obtain similar absorption cross-sections and molar extinction coefficients [20], which implies similar intensity of light absorbed (I_a), and so negligible differences regarding the number of excited electrons in the various PQDs was estimated. This similar I_a is one of the important factors for comparing radiative and non-radiative recombination kinetics for the various PQDs using different PbI_2 . In the perovskite, if the I_a and/or number of excited electrons would be different, major recombination-trap assisted recombination, bimolecular recombination of exciton/free carriers, or Auger recombination processes could be changed [21]. Furthermore, the similar sizes of PQDs (7–9 nm) demonstrate similar surface-to-volume ratios, which is one of the key factors that affects the number of surface defects in the PQDs. The surface defect density and surface defect induced non-radiative recombination kinetics could be changed by ligand, surface density [22], type of ligands [23,24], formation of core or core-shell structures [25,26], varying surface-to-volume ratios or sizes [27], and so on. However, in this study, we used the same QD structure, ligands, and their amounts for all synthetic

procedures of the PQDs. Therefore, the effect of ligands on PQD surface to non-radiative recombination kinetics could be experimentally controlled for all PQDs made using the four PbI_2 . Consequently, the observed PLQY and k_{nr} can be associated with defects associated with different characters of PbI_2 precursors with different I/Pb elemental ratio.

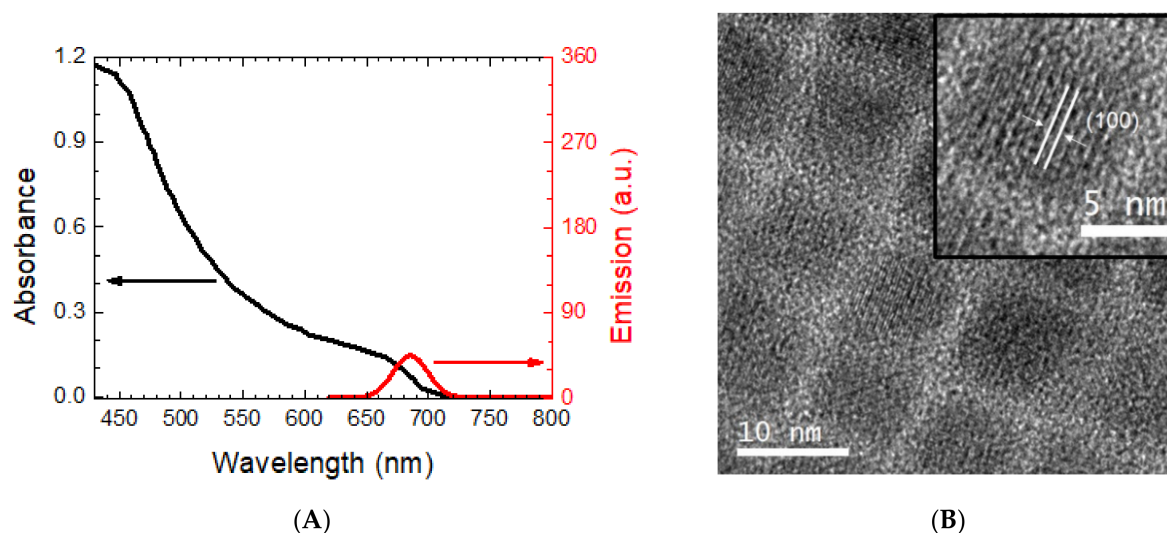


Figure 2. (A) UV-Vis. absorption (black line, left) and photoluminescence (red line, right) spectra of the CsPbI_3 PQDs, synthesized using Hot Water PbI_2 . (B) TEM image of the CsPbI_3 PQDs (inset: high resolution TEM image of single PQD with lattice fringe, which presents (100) plane of the CsPbI_3 structure).

To monitor the effect of the PbI_2 precursor purification on photophysical properties of CsPbI_3 PQDs, the four types of CsPbI_3 PQDs were synthesized using the four different PbI_2 (Commercial, As-synthesized, Ice Bath, and Hot Water PbI_2) and their PL spectra are shown in Figure 3A. Note that the emission spectra were taken from the PQD dispersed solutions by maintaining their absorbances at their absorption band edge around 0.1 ± 0.005 to obtain PLQY, as shown in Figure 3B. To obtain PLQY without dependency of degradation of the PQDs, the PLQY values were taken right after PQD synthesis in every time with comparisons of reference dye (riboflavin, see details in the Materials and Methods section) with the same absorbance at the band edge, through the following equation:

$$\Phi_{\text{PQD}} = \Phi_{\text{standard}} \times \frac{\text{Area}_{\text{PQD}}}{\text{Area}_{\text{standard}}} \times \frac{\eta_{\text{PQD}}^2}{\eta_{\text{standard}}^2} \quad (1)$$

In Equation (1), Φ_{PQD} , Φ_{standard} , Area_{PQD} , $\text{Area}_{\text{standard}}$, η_{PQD} , and η_{standard} represent PLQY of PQD, PLQY of standard dye (riboflavin), PL peak area of PQD, PL peak area of standard dye, refractive index of PQD dispersed solution (hexane), and refractive index of PQD dispersed solution (ethanol), respectively. PLQYs of PQDs using Commercial, As-synthesized, Ice Bath, and Hot Water PbI_2 are $52.3 \pm 5.2\%$, $61.8 \pm 5.6\%$, $81.3 \pm 7.7\%$, and $80.3 \pm 8.0\%$, respectively. In general, PLQY were assigned as follows:

$$\text{PLQY} = \frac{k_r}{k_r + k_{\text{nr}}} \quad (2)$$

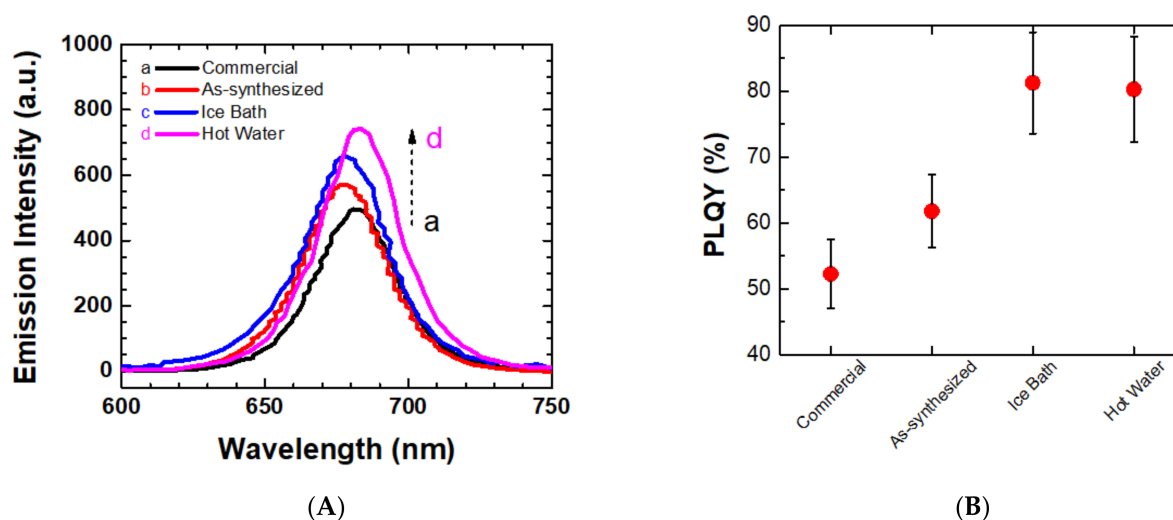


Figure 3. (A) Photoluminescence spectra of the four CsPbI₃ QDs made using four different PbI₂ (a: Commercial, b: As-synthesized, c: Ice Bath, d: Hot Water PbI₂). Photoluminescence spectra were taken by fixing their band edge absorption as 0.1 ± 0.005 . (B) PLQY of CsPbI₃ QDs made using four different PbI₂.

k_r represents the radiative recombination rate constant. In Figure 3A, emission intensities are higher for QDs using recrystallized PbI₂ precursors. Additionally, in Figure 3B, in the case of the QDs using recrystallized PbI₂, PLQYs were around 20% higher than QDs using As-synthesized PbI₂. The PLQY improvements could be concluded as decreasing k_{nr} due to following reasons: (1) similar intensity of light absorbed, I_a , using the same laser power excitation, which expects a similar number of excited electrons in the QDs, and (2) removal of impurity in the QDs, monitored through XRD patterns (see Figure S5). Especially, we speculate that the recrystallization of the PbI₂ precursor gives a positive effect to decrease iodide interstitial defects by giving better stoichiometry between I/Pb as 2.01–2.00 in QDs [16,18,19]. Note that detailed PLQY were obtained through Equation (1) by comparing emissions of riboflavin dye by matching fine absorption match and independent measurements right after QD synthesis to exclude the degradation effect, so it is hard to differentiate PLQY difference among $81.3 \pm 7.7\%$, and $80.3 \pm 8.0\%$. Furthermore, overall PLQYs are below 90%, by comparing early reported high PLQY values (>90%) [28] to the PLQY, there is still a significant impact from the non-radiative recombination process from charge trapping at the surface defect. More details could be investigated further regarding optimizing experimental QD synthetic conditions to increase overall PLQY. In short, the recrystallization process of precursor for QDs could contribute to providing qualified crystalline quality of the QDs and more emissive properties with higher PLQY.

To observe how recrystallization of the precursor affects the non-radiative recombination process in the QDs, time-correlated single photon counting (TCSPC) was performed to monitor time-resolved photoluminescence (TRPL) kinetic trace for the four CsPbI₃ QDs made using Commercial, As-synthesized, Ice Bath, and Hot Water PbI₂ (Figure 4 and Table 1). The averaged photoluminescence decay lifetimes (τ_{avg}) were obtained through a bi-exponential function fitting to the TRPL, as following Equation (3) [29]:

$$y = y_0 + A_1 e^{-x/\tau_1} + A_2 e^{-x/\tau_2} \quad (3)$$

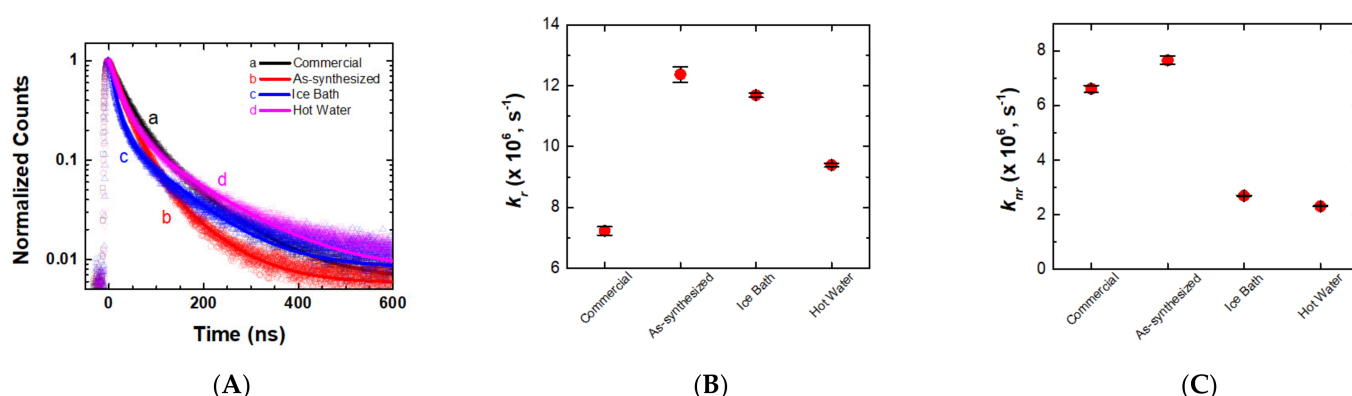


Figure 4. (A) Time-resolved photoluminescence decay kinetic traces of the four CsPbI₃ PQDs made using (a) Commercial, (b) As-synthesized, (c) Ice Bath, (d) Hot Water PbI₂, and their (B) k_r and (C) k_{nr} .

Table 1. Averaged photoluminescence decay lifetime (τ_{avg}), PLQY, k_r , and k_{nr} for the four CsPbI₃ PQDs made using the Commercial, As-synthesized, Ice Bath, and Hot Water PbI₂.

PbI ₂	τ_{avg} (ns)	PLQY (%)	k_r (s ⁻¹)	k_{nr} (s ⁻¹)
Commercial	72.3 ± 1.4	52.3 ± 5.2	7.23 ± 0.14 (×10 ⁶)	6.61 ± 0.13 (×10 ⁶)
As-synthesized	50.0 ± 1.0	61.8 ± 5.6	1.24 ± 0.03 (×10 ⁷)	7.64 ± 0.16 (×10 ⁶)
Ice Bath	69.5 ± 0.4	81.3 ± 7.7	1.17 ± 0.07 (×10 ⁷)	2.70 ± 0.02 (×10 ⁶)
Hot Water	85.5 ± 0.6	80.3 ± 8.0	9.39 ± 0.07 (×10 ⁶)	2.31 ± 0.02 (×10 ⁶)

In Figure 4A, the emission intensities were monitored with time delay. A_i and τ_i demonstrate weighted coefficients for each component and their time constants, respectively. The multi-exponential decay behavior of the PQDs was attributed to various fluctuations in the non-radiative recombination process, which include quenching of the excited electrons to trap sites [29,30]. In Table S1, the parameters through the fitting were demonstrated. The τ_{avg} were obtained through the following Equation (4) [29]:

$$\tau_{avg} = \frac{A_1\tau_1^2 + A_2\tau_2^2}{A_1\tau_1 + A_2\tau_2} \quad (4)$$

Overall, τ_{avg} for PQDs using recrystallized PbI₂ presented longer than τ_{avg} for PQDs using As-synthesized PbI₂ due to the bigger contribution of amplitude A_2 for longer time constants. The elongation of τ_{avg} is a result of decreasing k_r and/or k_{nr} , as follows [6]:

$$\tau_{avg} = \frac{1}{k_r + k_{nr}} \quad (5)$$

Through experiments, PLQY and τ_{avg} were obtained. Applying the PLQY and τ_{avg} values to Equations (2) and (5), k_r and k_{nr} were obtained and they are listed in Table 1. Interestingly, using recrystallized PbI₂ for the CsPbI₃ PQD synthesis decreases k_{nr} about 1/4 times slowly than the k_{nr} of PQDs using As-synthesized PbI₂ as precursor. Even though k_r also decreases 5.64% in the case of Ice Bath PbI₂ and 24.3% for the case of Hot Water PbI₂ (as compared to k_r for the case of using As-synthesized PbI₂), usage of recrystallized PbI₂ enabled us to retard k_{nr} (65% slower rate for Ice Bath and 70% slower rate for Hot Water, compared to the k_{nr} for As-synthesized) in the CsPbI₃ PQDs. It means that there is a positive correlation between recrystallization of PbI₂ as a precursor and retarding k_{nr} for favorable emission and reduction of the excited electron quenching at defect sites. We speculate that reduction of interstitial iodide in the perovskite could contribute to reducing the easily favored non-radiative recombination sites so that the relatively unfavored non-radiative recombination process retards the k_{nr} [16,18,19].

2.2. Halide Vacancy Mediated Surface Defect Passivation through Electrodeposition

To monitor reduction of excited electron trapping at surface defects and to occur favorable radiative recombination process, we also performed in situ PL spectroscopy while undergoing electrodeposition of CsPbBr₃/ITO film with positive voltage to cover the surface defects to bromide (Figure 5 and see details in Materials and Methods). In short, dispersed CsPbI₃ PQDs interacted with tetraoctylammonium bromide in the same solution phase. Under the ambient condition, CsPbBr₃ PQDs have better stability and form bulk CsPbBr₃ film following through annealing process to firmly attach on to the ITO substrate. In the films with positive applied bias (+0.6 V), the positive electric field attracted to bromide in the octylammonium bromide solution and deposited the bromide on the surface of the CsPbBr₃ perovskite layer. The +0.6 V corresponds to the relative higher energy level to valence band maximum of the perovskite and the energy level similarly matches to the halide vacancy and its hole mediated oxidation [18]. Note that the CsPbBr₃ perovskite film was surrounded by an octylammonium bromide solution so the electrical field in between the two electrodes made bromide move to the anode and octylammonium cation move to the cathode, instead of the hole-mediate oxidation under the electrical field. The quantitative movements of ion in between the electrodes and the accumulated number of electrons calculated through current are presented in Figure 5A. Under the constant applied bias, the current decreased while the electrodeposition occurred. We speculate that constant ion movements to the two electrodes (bromide to surface of the CsPbBr₃ perovskite and octylammonium cation to counter electrode) continuously decreased the overall concentration of the octylammonium bromide. However, the accumulated electron flow indicated that the successful electrodeposition of ions occurred and the successive bromide surface passivation on the CsPbBr₃ perovskite film surface occurred as well. Figure 5B demonstrates the emission enhancement during the electrodeposition process because of bromide passivation on the perovskite surface. Figure 5C presents electrodeposition-time based relative PLQY enhancement through the following equation, derived from Equation (1):

$$\frac{\Phi_t}{\Phi_0} = \frac{A_t}{A_0} \times \frac{\eta_t^2}{\eta_0^2} \quad (6)$$

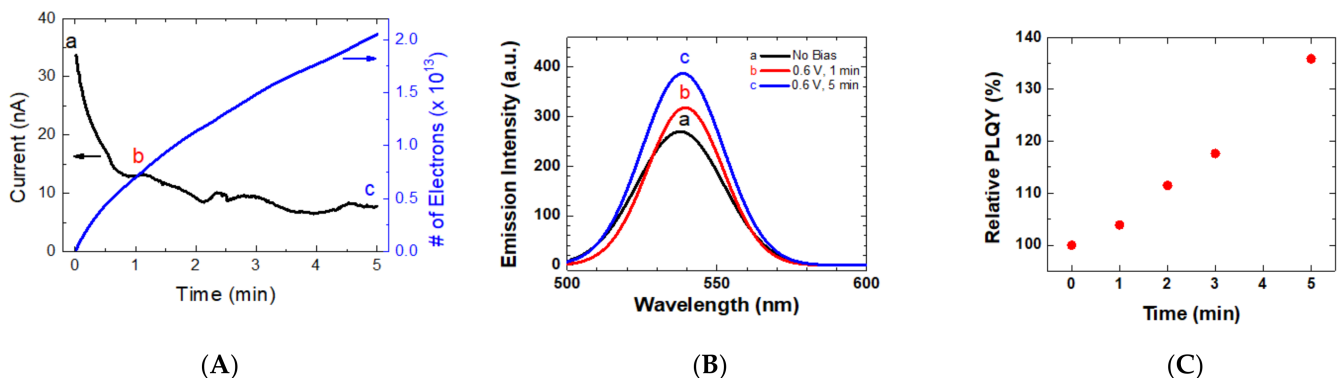


Figure 5. In situ photoluminescence spectra measurements under constant applied bias (+0.6 V) for electrodeposition of bromide on CsPbBr₃ perovskite film. (A) Current-time profiles and accumulated electron flow with time. (B) photoluminescence spectra of the CsPbBr₃ perovskite film during the moment assigned in (A). (C) Relative PLQY enhancement with comparison of (emission peak area at time)/(emission peak area at time zero without applied bias).

Φ_t , Φ_0 , A_t , A_0 , η_t , and η_0 represent PLQY of the CsPbBr₃ perovskite film at a certain time, PLQY of the CsPbBr₃ perovskite film at time zero, PL peak area of the CsPbBr₃ perovskite film at a certain time, PL peak area of the CsPbBr₃ perovskite film at time zero, the refractive index of the octylammonium bromide solution at a certain time, and the refractive index of the octylammonium bromide solution at time zero, respectively. Note that the change of refractive index of the octylammonium bromide solution under

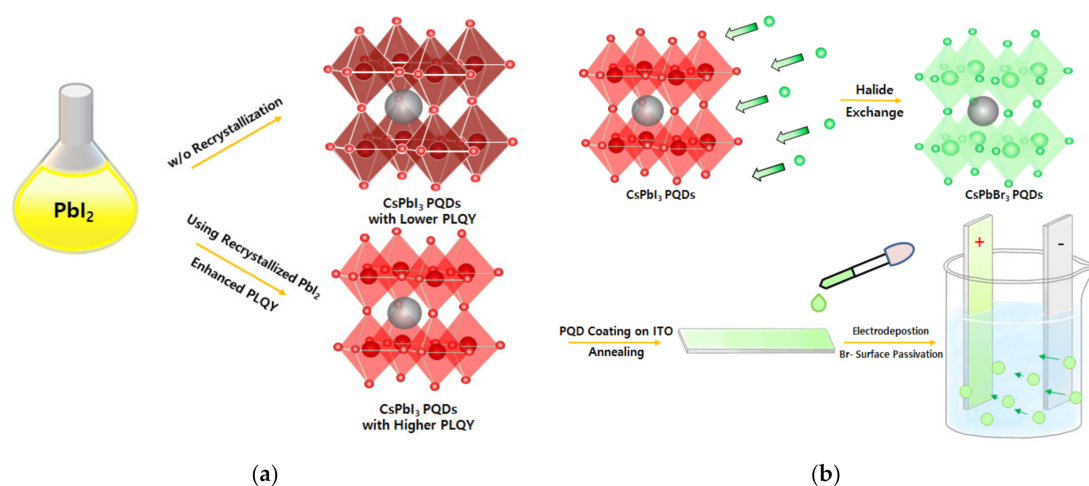
the electrodeposition process is negligible so $\frac{\eta_t^2}{\eta_0}$ in Equation (6) could be disregarded. Equation (6) could be simplified to Equation (7), as follows:

$$\frac{\phi_t}{\phi_0} = \frac{A_t}{A_0} \quad (7)$$

Therefore, through calculating the ratio between PL emission peak area at certain time and emission peak area at time zero, we present the relative PLQY change with the electrodeposition reaction time in Figure 5C. Note that the overall PLQY of CsPbBr₃ perovskite film is below 1% because efficient exciton separation occurs to form free carriers at room temperature due to similar energy values between exciton dissociation energy and thermal energy $k_B T \approx 25$ meV [11,23]. Additionally, dominant defect-mediated excited electron trapping induces the favorable non-radiative recombination process and so the favorable non-radiative recombination process also diminishes the overall PLQY of the perovskite film [11,23]. Furthermore, we also observed that there is a positive correlation between increasing applied electric field and emission enhancement (Figure S6). It means that the increased potential facilitates ion movement in the solution for the electrodeposition and so that the passivation of bromide on to the anode, perovskite film. Note that a similar electrodeposition technique could be performed for the PQD deposited film but by being placed in the electrolyte, both ion passivation and loss of PQD from film to electrolyte could be performed so that detailed experimental control could be issued. Through electrodeposition of bromide to perform bromide surface passivation on the CsPbBr₃ perovskite film, it could be possible to conclude that bromide surface passivation is one strategy to decrease non-radiative recombination processes at surface defects.

2.3. The Two Different Synthetic and Post-Synthetic Strategies to Improve Photoluminescence Quantum Yield of the PQDs

The two experimental strategies to control the non-radiative process at defects in the perovskite in this study are proposed in Scheme 1. First, recrystallization of the PbI₂ precursor positively affected the enhancement of the PLQY of CsPbI₃ PQDs due to removal of impurities in the PQD crystalline structure and retarding k_{nr} to increase the PLQY, following Equation (2). The purification of the precursor could positively affect the formation of PQDs with a lower number of defects so that the overall PLQY could be enhanced from 61.8% to 80.3%. The reason could be reduction of the interstitial iodide to induce favorable radiative recombination. Additionally, the post-synthetic process, electrodeposition, provided effective bromide surface passivation on the CsPbBr₃ perovskite film so that PLQY increased due to decreased excited electron quenching at defects, estimated by bromide vacancy. The bromide vacancy on the surface could also play a role in inducing a trapping site to the photoinduced excited electrons and further induce the non-radiative recombination process, which was detrimental for the PLQY.



Scheme 1. Two different strategies to obtain higher photoluminescence quantum yields. (a) With applying recrystallization process of PbI_2 precursor to enhance PLQY of PQDs. (b) Halide exchange to form from $CsPbI_3$ to $CsPbBr_3$ and subsequent annealing process to adhere $CsPbBr_3$ on ITO to apply the electrodeposition process to do halide surface defect passivation to decrease surface halide vacancy mediated non-radiative recombination process on the $CsPbBr_3$ perovskite film.

3. Materials and Methods

3.1. Materials

Lead acetate ($Pb(CH_3CO_2)_2$, 6080-56-4, 99.7%, Fisher Chemical, Waltham, MA, US), Potassium iodide (KI, 7681-11-0, 99.5%, Daejung Chemicals, Siheung-si, Korea), Hydrochloric acid (HCl, 7647-01-0, 35.0%, Daejung Chemicals, Siheung-si, Korea), Ethyl acetate (141-78-6, Duksan Chemicals, Ansan-si, Korea), n-octane (111-65-9, 97.0%, Daejung Chemicals, Siheung-si, Korea), Tetraoctylammonium bromide (14866-33-2, 98%, Sigma-Aldrich, Saint Louis, Missouri, US), Cs_2CO_3 , (Cs_2CO_3 , 534-17-8, 99.5%, Samchun Chemicals, Seoul, Korea), oleic acid (OA, 112-80-1, 90%, Alfa Aesar, Haverhill, US,), 1-octadecene (112-88-9, 90%, Sigma-Aldrich, Saint Louis, Missouri, US), PbI_2 (10101-63-0, 99%, Sigma-Aldrich, Saint Louis, Missouri, US), PbI_2 with higher purity (10101-63-0, 99.999%, TCI, Paris, France), and oleylamine (112-90-3, 50%, OLA, TCI, Paris, France)

3.2. Methods

3.2.1. Synthesis of the PbI_2 Perovskite Precursors and Recrystallization Process

First, 0.339 g lead acetate and 0.238 g potassium iodide were each dissolved in 100 mL of distilled water [6]. A total of 0.3 mL of 1 M Hydrochloric acid was added to the lead acetate solution to prevent hydrolysis. We simply mixed the two solutions with a few drops at an early moment. Soon, bright yellow lead iodide was produced. After the precipitate was formed, heat was applied to the solution to $\sim 80^\circ C$ in 1 h by putting the solution in a water bath to induce complete dissolution of PbI_2 . Then cooling applied either (1) or (2), as follows:

- (1) Recrystallization process with slow cooling (called “Hot Water”)

The heating was turned off and the solution was placed in the water bath. Gradual cooling down to room temperature occurred on its own (~ 2 h). After watching the crystals for around 2 h, the flask was kept in the lab fridge for 3 h to obtain as many crystals as possible, then the precipitation was filtered to isolate the lead iodide. The filtered lead iodide was dried under a vacuum overnight.

- (2) Recrystallization process with fast cooling (called “Ice”)

The heated solution was placed in a flask inside the ice bath in the lab fridge for 3 h to obtain as many crystals as possible. Then, the crystallized lead iodide was filtered, and dried under vacuum overnight.

3.2.2. Synthesis of CsPbI₃ Perovskite Quantum Dots

The synthetic procedure for CsPbI₃ perovskite quantum dots was from our previous work [3,6,31]. In brief, a mixture composed of 0.407 g of Cs₂CO₃, 1.25 mL of oleic acid, and 20 mL of 1-octadecene was degasified in a 50 mL three neck flask under vacuum for 30 min at 80 °C, under vacuum for 30 min at 120 °C, and then heated at 140 °C under N₂ conditions until Cs₂CO₃ reacted completely with OA. A translucent clear Cs-oleate solution was achieved. Before injection, the solution was preheated at 115 °C, keeping the N₂-purging, to avoid the precipitation of Cs-oleate. Note that the appearance of a dark orange color in the Cs-oleate solution is indicative of Cs-oleate oxidation to form Cs₂O.

To synthesize CsPbI₃ quantum dots, 0.5 g of PbI₂ was mixed with 50 mL of 1-ODE in a 100 mL three neck flask. The mixture was dried under vacuum at 120 °C for 30 min. Then, preheated OA and OAm (2.5 mL of each) were loaded in the solution at 130 °C, and briefly it was degasified until the complete dissolution of precursors.

Under N₂-purging, the temperature of reaction was raised to 170 °C, and 2 mL of Cs-oleate solution was quickly injected. Lastly, the reaction was quenched after adding the reaction flask in an ice bath until a fall in temperature in the range of 60–70 °C.

3.2.3. Halide Exchange Process and Deposition of Perovskite Quantum Dots and on ITO to form Stable CsPbBr₃ Perovskite/ITO Films in Ambient Condition at Room Temperature

First, halide exchange was performed by reacting 2 mL CsPbI₃ PQDs with 0.2 g tetraoctylammonium bromide under vigorous stirring. We obtained the supernatant, CsPbBr₃ PQD. A total of 3 mL ethyl acetate was added to 1.5 mL halide exchange QDs solution and then centrifuged at 6000 rpm for 20 min. The supernatant was discarded, and the QDs was dispersed again in 1 mL hexane and then 300 rpm 3 min. Dispersed solutions were taken and N₂ blow applied for 10 min to remove hexane solvent. The remained PQDs were dispersed in 2 mL n-octane. The PQD dispersed octane solution was drop-cast on ITO and dried under N₂ gas flow. To form CsPbBr₃ bulk film, the drop-cast PQD/ITO film was annealed at 225 °C for 3 min, under ambient condition, as reported in earlier literature [31].

3.2.4. Characterizations

The steady state absorption spectra of colloidal CsPbI₃ quantum dot solutions and films were achieved by using a UV/Vis absorption and photoluminescence spectrophotometer (Lab junior, K-MAC) by using a 450 nm LED light source (power density ~1 mW/cm²). The in situ changes of the absorption/emission features of the CsPbBr₃ perovskite films were monitored with a CCD camera with and without applied bias (WPG100e potentiostat/galvanostat, Wonatech). In addition, combining incident photon-to-electron conversion efficiency (IPCE) setup, charge-coupled devices (CCD) detector, and additional optic tools, we prepared a homemade setup (as IPCE-CCD) for in situ absorption/emission measurement with and without applied bias during the electrodeposition process. The CsPbBr₃ perovskite/ITO films were connected to the anode and dipped in an octylammonium bromide isopropanol solution (100 mg/mL). Another ITO film was used as a counter electrode. Various neutral density filters were applied in front of the detector to control overall emission intensity incoming to the detector.

Lead iodide crystal structure was measured using X-ray diffraction (XRD) analysis (XRD, Mini Flex 600, Rigaku). The perovskite quantum dot crystal structure was measured using a field emission transmission electron microscope (FE-TEM, Tecnai G2 F20 S-TWIN, FEI Korea). The relative PLQY of the quantum dots were obtained by comparing emission from riboflavin dye [6]. TRPL were measured through TCSPC (Fluotime 300, PicoQuant, Berlin, Germany) with 520 nm pulse laser excitation (pulse duration < 100 ps). Elemental analysis of PbI₂ was characterized through an energy-dispersive X-ray fluorescence spectrometer (PanalyticalEpsilon, 3-XLE, Malvern, UK) at the Core Research Support Center for Natural Products and Medical Materials at Yeungnam University.

4. Conclusions

We presented two strategies for higher PLQY of the perovskites by using i) higher quality PbI_2 with better I/Pb stoichiometric ratios to decrease iodide interstitials in the PQDs and ii) using the electrodeposition technique to passivate halide surface vacancies. The recrystallized PbI_2 precursors for perovskite improved the quality of the PQDs for two reasons. First, the XRD patterns of the PbI_2 precursors provided a positive role in the recrystallization process to remove impurities. Second, XRF confirmed enhanced I/Pb stoichiometry in the PbI_2 from applying the recrystallization process. Using recrystallized PbI_2 contributed to enhancing the PLQY of PQD from 62% to over 80% due to enriched iodine synthetic atmosphere, which implies decreased iodide-based interstitial defects. Additionally, the recrystallized PbI_2 improved PQD synthetic quality with diminished byproducts, monitored XRD patterns of PQDs made with and without using the recrystallized PbI_2 . TCSPC results supports selectively retarded k_{nr} with a four times slower rate by applying the additional recrystallization process. Furthermore, to study the role of halide vacancy mediated defects, we prepared the CsPbBr_3 film on ITO using halide exchange (bromide to iodide) and subsequent annealing process to form agglomerated bulk morphology on ITO [32]. Under the applied bias, we observed the positive correspondence between current as results of halide movements in the solution and deposition on the anode (CsPbBr_3 film), and enhancement of PL. The correspondence implies that the surface passivation of halide-mediated defects suppresses the halide vacancy mediated non-radiative recombination sites. Therefore, these two different strategies to control defects could contribute to how conventional chemistry techniques applied to the modern renewable energy research field can enhance the photophysical properties of the key materials for the next generation, such as perovskite. This work could open both fundamentals of halide defect chemistry for perovskites and practical challenges to improve the performance of optoelectronic devices.

Supplementary Materials: The following are available online at <https://www.mdpi.com/article/10.3390/catal11080957/s1>, Figure S1: Schematic images of PbI_2 precipitation method, Figure S2: XRD pattern of PbI_2 with 99.999% purity, Figure S3: UV-visible absorption spectra (A) and photoluminescence spectra (B) of CsPbI_3 PQD dispersed solutions. Four different PQDs were synthesized using Commercial (black line), As-synthesized (red line), Ice Bath (blue line), and Hot Water (purple line) PbI_2 as precursor, Figure S4: TEM images for the four different CsPbI_3 PQDs and their size histograms: PQDs made using Commercial (A,B), As-synthesized (C,D), Ice Bath (E,F), and Hot Water (G,H) PbI_2 as precursors, Figure S5: XRD patterns of the four different CsPbI_3 PQDs: PQDs made using Commercial (black line), As-synthesized (red line), Ice Bath (blue line), and Hot Water (purple line) PbI_2 as precursors. Peak assignment was referred from pdf number 161481, Figure S6: in-situ photoluminescence spectra of CsPbBr_3 perovskite film under applying bias with gradually increasing voltage from 0 to 50 V, Table S1: XRF elemental results about Pb and I and their molar ratio (I/Pb) for Commercial, As-synthesized, Ice Bath, and Hot Water PbI_2 , Table S2: Results of bi-exponential fitting for time-resolved photoluminescence kinetic traces of the four different CsPbI_3 PQD dispersed solutions. All authors have read and agreed to the published version of the manuscript.

Author Contributions: S.J.Y. and A.F.G.-R. designed the experiments. I.M.-S. and S.-H.H. discussed implications of different characterization. S.J.Y., C.L., S.J.L., Y.S. and Y.W. performed the experiments. All authors contributed to analysis of the results, data analysis, and preparation of the final manuscript. Furthermore, the authors, C.L. and S.J.L. are equally contributed to this work. All authors have read and agreed to the published version of the manuscript.

Funding: This work was supported by the National Research Foundation of Korea (NRF) grant funded by the Korean government (MSIT) 2019R1F1A1062395 and 2021R1F1A1063382. This work was also supported by the X-mind Corps program of the National Research Foundation of Korea 32(NRF) funded by the Ministry of Science, ICT (2019H1D8A1105630). This work was partially supported by the Ministry of Science and Innovation of Spain under Project STABLE (PID2019-107314RB-I00), Generalitat Valenciana via Prometeo Grant Q-Devices (Prometeo/2018/098).

Acknowledgments: We thank the Core Research Support Center for Natural Products and Medical Materials (CRCNM) for technical support regarding the energy-dispersive X-ray fluorescence spectrometer (PanalyticalEpsilon, 3-XLE).

Conflicts of Interest: The authors declare no conflict of interest.

References

1. Protesescu, L.; Yakunin, S.; Bodnarchuk, M.I.; Krieg, F.; Caputo, R.; Hendon, C.H.; Yang, R.X.; Walsh, A.; Kovalenko, M.V. Nanocrystals of Cesium Lead Halide Perovskites (CsPbX_3 , X = Cl, Br, and I): Novel Optoelectronic Materials Showing Bright Emission with Wide Color Gamut. *Nano Lett.* **2015**, *15*, 3692–3696. [CrossRef]
2. Kim, G.; Min, H.; Lee, K.S.; Lee, D.Y.; Yoon, S.M.; Seok, S.I. Impact of Strain Relaxation on Performance of Alpha-formamidinium Lead Iodide Perovskite Solar Cells. *Science* **2020**, *370*, 108–112. [CrossRef]
3. Gualdrón-Reyes, A.F.; Yoon, S.J.; Barea, E.M.; Agouram, S.; Munoz-Sanjose, V.; Melendez, A.M.; Nino-Gomez, M.E.; Mora-Sero, I. Controlling the Phase Segregation in Mixed Halide Perovskites through Nanocrystal Size. *ACS Energy Lett.* **2019**, *4*, 54–62. [CrossRef] [PubMed]
4. Zhang, Y.; Kim, S.G.; Lee, D.K.; Park, N.G. $\text{CH}_3\text{NH}_3\text{PbI}_3$ and $\text{HC}(\text{NH}_2)_2\text{PbI}_3$ Powders Synthesized from Low-Grade PbI_2 : Single Precursor for High-Efficiency Perovskite Solar Cells. *ChemSuschem* **2018**, *11*, 1813–1823. [CrossRef] [PubMed]
5. Kim, J.; Park, B.W.; Baek, J.; Yun, J.S.; Kwon, H.W.; Seidel, J.; Min, H.; Coelho, S.; Lim, S.; Huang, S.J.; et al. Unveiling the Relationship between the Perovskite Precursor Solution and the Resulting Device Performance. *J. Am. Chem. Soc.* **2020**, *142*, 6251–6260. [CrossRef] [PubMed]
6. Lee, C.; Shin, Y.; Jeon, G.G.; Kang, D.; Jung, J.; Jeon, B.; Park, J.; Kim, J.; Yoon, S.J. Cost-efficient, Effect of Low-Quality PbI_2 Purification to Enhance Performances of Perovskite Quantum Dots and Perovskite Solar Cells. *Energies* **2021**, *14*, 201.
7. Yuan, Y.; Huang, J. Ion Migration in Organometal Trihalide Perovskite and Its Impact on Photovoltaic Efficiency and Stability. *Acc. Chem. Res.* **2016**, *49*, 286–293. [CrossRef]
8. Jeon, N.J.; Noh, J.H.; Kim, Y.C.; Yang, W.S.; Ryu, S.; Seok, S.I. Solvent Engineering for High-performance Inorganic-organic Hybrid Perovskite Solar Cells. *Nat. Mater.* **2014**, *13*, 897–903. [CrossRef]
9. Tress, W.; Yavari, M.; Domanski, K.; Yadav, P.; Niesen, B.; Correa Baena, J.P.; Hagfeldt, A.; Graetzel, M. Interpretation and Evolution of Open-circuit Voltage, Recombination, Ideality Factor and Subgap Defect States During Reversible Light-soaking and Irreversible Degradation of Perovskite Solar Cells. *Energy Environ. Sci.* **2018**, *11*, 151–165. [CrossRef]
10. Zolfaghari, Z.; Hassanabadi, E.; Pitarch-Tena, D.; Yoon, S.J.; Shariatnia, Z.; van de Lagemaat, J.; Luther, J.M.; Mora-Sero, I. Operation Mechanism of Perovskite Quantum Dot Solar Cells Probed by Impedance Spectroscopy. *ACS Energy Lett.* **2019**, *4*, 251–258. [CrossRef]
11. Sum, T.C.; Mathews, N.; Xing, G.; Lim, S.S.; Chong, W.K.; Giovanni, D.; Dewi, H.A. Spectral Features and Charge Dynamics of Lead Halide Perovskites: Origins and Interpretations. *Acc. Chem. Res.* **2016**, *49*, 294–302. [CrossRef] [PubMed]
12. Christians, J.A.; Leighton, D.T.; Kamat, P.V. Rate Limiting Interfacial Hole Transfer in Sb_2S_3 Solid-state Solar Cells. *Energy Environ. Sci.* **2014**, *7*, 1148–1158. [CrossRef]
13. Konidakis, I.; Maksudov, T.; Serpetzoglou, E.; Kakavelakis, G.; Kymakis, E.; Stratakis, E. Improved Charge Carrier Dynamics of $\text{CH}_3\text{NH}_3\text{PbI}_3$ Perovskite Films Synthesized by Means of Laser-Assisted Crystallization. *ACS Appl. Energy Mater.* **2018**, *1*, 5101–5111. [CrossRef]
14. Li, F.; Zhu, W.; Bao, C.; Yu, T.; Wang, Y.; Zhou, X.; Zou, Z. Laser-assisted crystallization of $\text{CH}_3\text{NH}_3\text{PbI}_3$ Films for Efficient Perovskite Solar Cells with a High Open-circuit Voltage. *Chem. Commun.* **2016**, *52*, 5394–5397. [CrossRef]
15. Gualdrón-Reyes, A.F.; Masi, S.; Mora-Seró, I. Progress in Halide-perovskite Nanocrystals with Near-unity Photoluminescence Quantum Yield. *Trends Chem.* **2021**, *3*, 499–511. [CrossRef]
16. Huang, H.; Bodnarchuk, M.I.; Kershaw, S.V.; Kovalenko, M.V.; Rogach, A.L. Lead Halide Perovskite Nanocrystals in the Research Spotlight: Stability and Defect Tolerance. *ACS Energy Lett.* **2017**, *2*, 2071–2083. [CrossRef]
17. Golden Rain. Available online: <https://edu.rsc.org/exhibition-chemistry/golden-rain/2000048.article> (accessed on 20 December 2020).
18. Samu, G.F.; Balog, A.; De Angelis, F.; Meggiolaro, D.; Kamat, P.V.; Janaky, C. Electrochemical Hole Injection Selectively Expels Iodide from Mixed Halide Perovskite Films. *J. Am. Chem. Soc.* **2019**, *141*, 10812–10820. [CrossRef]
19. Buin, A.; Pietsch, P.; Xu, J.; Voznyy, O.; Ip, A.H.; Comin, R.; Sargent, E.H. Materials Processing Routes to Trap-free Halide Perovskites. *Nano Lett.* **2014**, *14*, 6281–6286. [CrossRef]
20. Wang, C.; Chesman, A.S.R.; Yin, W.; Frazer, L.; Funston, A.M.; Jasieniak, J.J. Facile Purification of CsPbX_3 (X = Cl^- , Br^- , I^-) Perovskite Nanocrystals. *J. Chem. Phys.* **2019**, *151*, 121105. [CrossRef]
21. Draguta, S.; Thakur, S.; Morozov, Y.V.; Wang, Y.; Manser, J.S.; Kamat, P.V.; Kuno, M. Spatially Non-uniform Trap State Densities in Solution-Processed Hybrid Perovskite Thin Films. *J. Phys. Chem. Lett.* **2016**, *7*, 715–721. [CrossRef] [PubMed]
22. Hines, D.A.; Becker, M.A.; Kamat, P.V. Photoinduced Surface Oxidation and Its Effect on the Exciton Dynamics of CdSe Quantum Dots. *J. Phys. Chem. C* **2012**, *116*, 13452–13457. [CrossRef]
23. Manser, J.S.; Christians, J.A.; Kamat, P.V. Intriguing Optoelectronic Properties of Metal Halide Perovskites. *Chem. Rev.* **2016**, *116*, 12956–13008. [CrossRef]
24. Hines, D.A.; Kamat, P.V. Quantum Dot Surface Chemistry: Ligand Effects and Electron Transfer Reactions. *J. Phys. Chem. C* **2013**, *117*, 14418–14426. [CrossRef]

25. Bridewell, V.L.; Alam, R.; Karwacki, C.J.; Kamat, P.V. CdSe/CdS Nanorod Photocatalysts: Tuning the Interfacial Charge Transfer Process through Shell Length. *Chem. Mater.* **2015**, *27*, 5064–5071. [[CrossRef](#)]
26. Dabbousi, B.O.; Rodríguez-Viejo, J.; Mikulec, F.V.; Heine, J.R.; Mattoussi, H.; Ober, R.; Jensen, K.F.; Bawendi, M.G. (CdSe)ZnS Core-shell Quantum Dots: Synthesis and Characterization of a Size Series of Highly Luminiscent Nanocrystallines. *J. Phys. Chem. B* **1997**, *101*, 9463. [[CrossRef](#)]
27. Kahmann, S.; Sytnyk, M.; Schrenker, N.; Matt, G.J.; Spiecker, E.; Heiss, W.; Brabec, C.J.; Loi, M.A. Revealing Trap States in Lead Sulphide Colloidal Quantum Dots by Photoinduced Absorption Spectroscopy. *Adv. Electron. Mater.* **2018**, *4*, 1700348. [[CrossRef](#)]
28. Hassanabadi, E.; Latifi, M.; Gualdrón-Reyes, A.F.; Masi, S.; Yoon, S.J.; Poyatos, M.; Julián-López, B.; Mora-Seró, I. Ligand & Band Gap Engineering: Tailoring the Protocol Synthesis for Achieving High-quality CsPbI₃ Quantum Dots. *Nanoscale* **2020**, *12*, 14194–14203.
29. Yoon, S.J.; Guo, Z.; Claro, P.C.D.; Sheychenko, E.V.; Huang, L.B. Direct Imaging of Long-Range Exciton Transport in Quantum Dot Superlattices by Ultrafast Microscopy. *ACS Nano* **2016**, *10*, 7208–7215. [[CrossRef](#)] [[PubMed](#)]
30. Fisher, B.R.; Eisler, H.-J.; Stott, N.E.; Bawendi, M.G. Emission Intensity Dependence and Single-Exponential Behavior In Single Colloidal Quantum Dot Fluorescence Lifetimes. *J. Phys. Chem. B* **2004**, *108*, 143–148. [[CrossRef](#)]
31. Lee, C.; Kim, K.; Shin, Y.; Han, D.; Yoon, S.J. In Situ Spectroelectrochemical Investigation of Perovskite Quantum Dots for Tracking Their Transformation. *Front. Energy Res.* **2021**, *8*. [[CrossRef](#)]
32. Hoffman, J.B.; Zaiats, G.; Wappes, I.; Kamat, P.V. CsPbBr₃ Solar Cells: Controlled Film Growth through Layer-by-Layer Quantum Dot Deposition. *Chem. Mater.* **2017**, *29*, 9767–9774. [[CrossRef](#)]